



Fe-doped $\text{In}_2\text{O}_3/\alpha\text{-Fe}_2\text{O}_3$ core/shell nanofibers fabricated by using a co-electrospinning method and its magnetic properties



Bon-Ryul Koo^a, Il-Kyu Park^{b,*}, Hyo-Jin Ahn^{a,*}

^a Department of Materials Science and Engineering, Seoul National University of Science and Technology, Seoul 139-743, Republic of Korea

^b Department of Electronic Engineering, Yeungnam University, Gyeongsbuk 712-749, Republic of Korea

ARTICLE INFO

Article history:

Received 4 February 2014

Received in revised form 11 March 2014

Accepted 11 March 2014

Available online 20 March 2014

Keywords:

Fe-doped In_2O_3

$\alpha\text{-Fe}_2\text{O}_3$

Nanofiber

Co-electrospinning

Core/shell nano-structure

ABSTRACT

We report on the fabrication and magnetic properties of Fe-doped $\text{In}_2\text{O}_3/\alpha\text{-Fe}_2\text{O}_3$ core/shell nanofibers (NFs) by co-electrospinning method. The structural investigations showed that the core and shell materials were composed of crystalline Fe-doped In_2O_3 NFs and $\alpha\text{-Fe}_2\text{O}_3$ nanoparticles with a size of less than 1 μm , respectively, and the morphologies of the resultant NFs changed with variation of the relative source ratio of In to Fe (the In/Fe molar ratio). Interestingly, X-ray diffraction and X-ray photoelectron spectroscopy results showed that the Fe elements were incorporated into the In_2O_3 lattice, causing a modification of the magnetic properties of the $\text{In}_2\text{O}_3/\alpha\text{-Fe}_2\text{O}_3$ core/shell NFs. Investigations of the magnetic properties of the core/shell NFs showed enhanced magnetic properties, and an increase in saturation magnetization values with an increased In/Fe molar ratio. Based on our results, we suggest three mechanisms for the enhancement of magnetic properties that result from our proposed structures.

© 2014 Elsevier B.V. All rights reserved.

1. Introduction

Magnetic nano-materials are of great technological importance for many applications including high-density magnetic recording media [1], bio-materials for magnetic separation and drug delivery [2,3], spintronics [4], magneto-optics [5], ferrofluids [6], magnetic resonance imaging [7], and various catalysts [8]. Controlling the size and structure of nano-materials offers many advantages due to additional options for size, and shape-dependent magnetic properties, excluding their intrinsic material properties. Among the magnetic materials, $\alpha\text{-Fe}_2\text{O}_3$ has been widely investigated because of its unique *n*-type semiconducting and antiferromagnetism properties, and for its numerous industrial applications for magnetic devices, pigments, and lithium ion batteries [9,10]. Therefore, many approaches to fabricating high quality $\alpha\text{-Fe}_2\text{O}_3$ nano-materials with various shapes of nanoparticle, nanocube, nanorod, nanobelt, nanotube, and nanoflake have been reported including hydrothermal [11], solvo-thermal [12], and forced hydrolysis methods [13]. However, the magnetic properties of fabricated $\alpha\text{-Fe}_2\text{O}_3$, such as saturation magnetization and coercivity, are still inadequate for commercial applications [9–13]. In addition, as

the resulting products are nano-sized powder form, their surfaces are easily degraded and agglomerated [9–13]. This results in a modification of the magnetic properties due to the exchange-bias effect. Therefore, developing a simplified and productive method to fabricate stable magnetic nano-materials is needed for commercial applications. In particular, electrospinning is one of attractive methods for preparing 1-dimensional (1-D) nanostructures including polymers, composites, and metal oxides because it has advantages such as large-scale productivity, simplicity, and low-cost [14–16]. Because 1-D nanostructures affect the performance of the magnetic property, electrospinning have attracted considerable interest for fabricating the various magnetic materials [17,18]. For example, Pan et al. synthesized NiFe_2O_4 nanofibers with diameters of 100 nm using electrospinning and demonstrated that NiFe_2O_4 nanofibers possess superb saturation magnetization (M_s) of 57.6 emu/g due to shape anisotropy [17]. Lee et al. reported that LaFe_2O_4 nanofibers prepared using electrospinning exhibited ferromagnetic properties with a coercivity of 28,078 Oe and a remnant magnetization of 0.23 emu/g [18]. However, few has been reported about the fabrication of $\alpha\text{-Fe}_2\text{O}_3$ with enhanced magnetic properties with 1-D nanostructures based on the electrospinning method. In this study, we report on the fabrication of Fe-doped $\text{In}_2\text{O}_3/\alpha\text{-Fe}_2\text{O}_3$ nanofibers (NFs) with enhanced magnetic properties by using a co-electrospinning method.

* Corresponding authors. Tel.: +82 538103093, 029706622; fax: +82 029736657, 538104770.

E-mail addresses: ikpark@ynu.ac.kr (I.-K. Park), hjahn@seoultech.ac.kr (H.-J. Ahn).

2. Experimental

As a reference for core/shell NFs, single α - Fe_2O_3 NFs were synthesized by electrospinning. Iron (III) nitrate nonahydrate [$\text{Fe}(\text{NO}_3)_3 \cdot 9\text{H}_2\text{O}$, Sigma–Aldrich] and poly(vinylpyrrolidone) (PVP, $M_w = 13,00,000$ g/mol, Sigma–Aldrich) were dissolved in N,N-dimethylformamide (DMF, Sigma–Aldrich) with stirring. This solution was loaded into a syringe equipped with a 23 gauge needle. The feeding rate was maintained at ~ 0.01 mL/h. Also, the distance between the needle and the collector, and the voltage were fixed at ~ 17 cm and 18 kV, respectively, finally obtaining the as-spun α - Fe_2O_3 NFs (hereafter referred to as sample A). In addition, Fe-doped $\text{In}_2\text{O}_3/\alpha$ - Fe_2O_3 core/shell NFs were synthesized by using a co-electrospinning method [19]. As shown in Fig. 1(a), the co-electrospinning apparatus consisted of a collector, power supply, syringe pump, syringe, and needle. In particular, the needle used for co-electrospinning was divided into core and shell regions. Owing to above-mentioned structures, it was possible to fabricate the core/shell NFs by using two different solutions. For the core region, indium (III) chloride tetrahydrate ($\text{InCl}_4\text{H}_2\text{O}$, Sigma–Aldrich) dissolved in ethanol ($\text{CH}_3\text{CH}_2\text{OH}$, Sigma–Aldrich) and PVP ($M_w = 3,60,000$ g/mol, Sigma–Aldrich) dissolved in a mixture solution of DMF and ethanol and were stirred for 1 h. For the shell region, iron (III) nitrate nonahydrate was dissolved in DMF and PVP and was stirred for 1 h. To investigate the morphological and characteristic evolution of the core/shell NFs, the relative molar ratio of In precursor to Fe precursor (In/Fe molar ratio) was adjusted to 0.5, 1, and 2 (hereafter referred to as samples B, C, and D, respectively). For electrospinning, the prepared solutions were transferred into each syringe using a 26 gauge needle for the core region and an 18 gauge needle for the shell region, respectively. The experimental conditions were the same as in the aforementioned procedures. As-spun NFs before calcination consisted of In metal precursor-PVP composite NFs for the core region and Fe metal precursor-PVP composite NFs for the shell region, respectively. During the calcination process, the as-spun NFs were heat-treated at 500°C for 5 h in order to obtain oxide-based NFs, and to remove the residual polymer. As a result, three different types of Fe-doped $\text{In}_2\text{O}_3/\alpha$ - Fe_2O_3 core/shell NFs were synthesized after calcination. Fig. 1 shows schematics for the fabrication of the Fe-doped $\text{In}_2\text{O}_3/\alpha$ - Fe_2O_3 core/shell NFs using the co-electrospinning method.

2.1. Characterizations

Structural and chemical investigations were performed using X-ray diffraction (XRD, Rigaku D/Max-2500 diffractometer using $\text{Cu K}\alpha$ radiation) and X-ray photoelectron spectroscopy (XPS, ESCALAB 250 equipped with an $\text{Al K}\alpha$ X-ray source), respectively. The morphological evolution of the samples was characterized by field-emission scanning electron microscopy (FE-SEM, Hitachi S-4700) and multifunctional transmission electron microscopy (MULTI/TEM; Tecnai G^2) with energy dispersive X-ray spectroscopy (EDS; Thermo NORAN System 7). The magnetic properties of the samples were measured at 300 K using a vibrating sample magnetometer (VSM; MicroSense, EV9).

3. Results and discussion

Fig. 2 shows FE-SEM images of the single Fe_2O_3 NF (sample A) and core/shell $\text{In}_2\text{O}_3/\text{Fe}_2\text{O}_3$ NFs (samples B–D) fabricated by using co-electrospinning after calcination at 500°C . All samples show continuous one-dimensional (1-D) NFs with a wax bean shape. The average diameters of the samples are ~ 97.7 nm for sample A, ~ 107.2 nm for sample B, ~ 136.3 nm for sample C, and ~ 103.5 nm for sample D. These results show that the NFs were successfully synthesized by the proposed co-electrospinning method. Sample A, synthesized by only Fe source, shows continuous NFs with small domains. And samples B, C, and D, synthesized

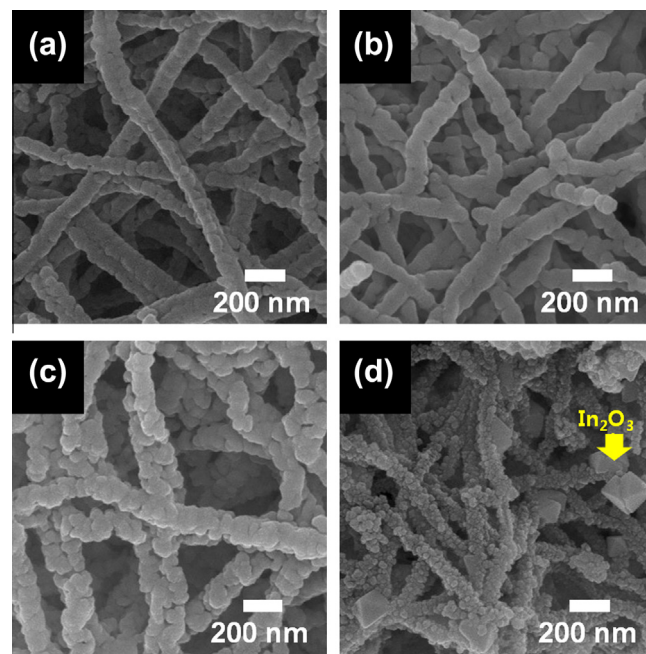


Fig. 2. Structural morphological evolutions with variation of the source Fe/In ratio. (a) Sample A, (b) sample B, (c) sample C and (d) sample D.

by co-electrospinning with the Fe and In sources, show small particles attached to NFs. The size of the nanoparticles on the NF surfaces increased by increasing the In/Fe molar ratio of samples B and C. In particular, for an In/Fe molar ratio of 2 (sample D), few octahedron-shaped particles with a size of ~ 200 nm were found on the surface of NFs. It has been reported that a single crystalline In_2O_3 with octahedral shape can be easily formed when an In metal is under an oxidation atmosphere at high temperature [20]. The crystalline structure of In_2O_3 , bixbyite, is usually cubes and its corners can be modified by octahedral faces to form an octahedron. Therefore, we assume that these octahedron particles can be a single crystalline In_2O_3 . Although the In_2O_3 was used as a core material in co-electrospinning, octahedral-shaped In_2O_3 particles were found on the surfaces of the NFs. This is due to precipitation and oxidation of the In metals during the thermal annealing process, or to the Ostwald ripening growth mechanism as a result of an excessive amount of In precursor in the core area [21]. The effect of these structural properties on the magnetic property of the NFs was investigated and will be discussed later.

Fig. 3(a)–(d) shows TEM images for samples A, B, C, and D, respectively. Sample A shows only Fe_2O_3 NF, which has a tubular shape because no core material was injected into the electrospinning syringe. The shell area of the NFs is composed of small

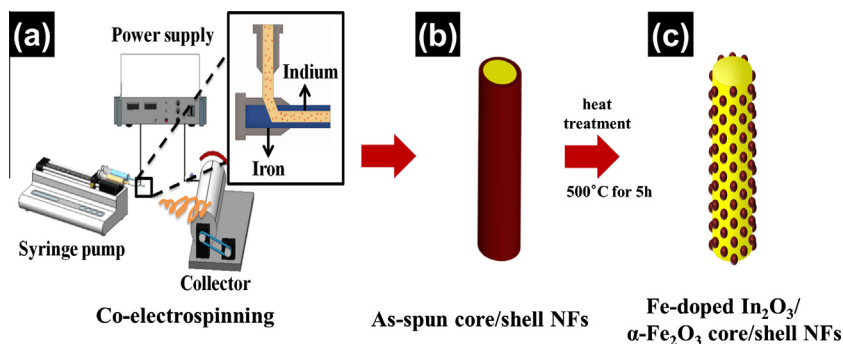


Fig. 1. Schematic diagram for the fabrication of Fe-doped $\text{In}_2\text{O}_3/\alpha$ - Fe_2O_3 core/shell NFs using co-electrospinning, and the resulting NF structure.

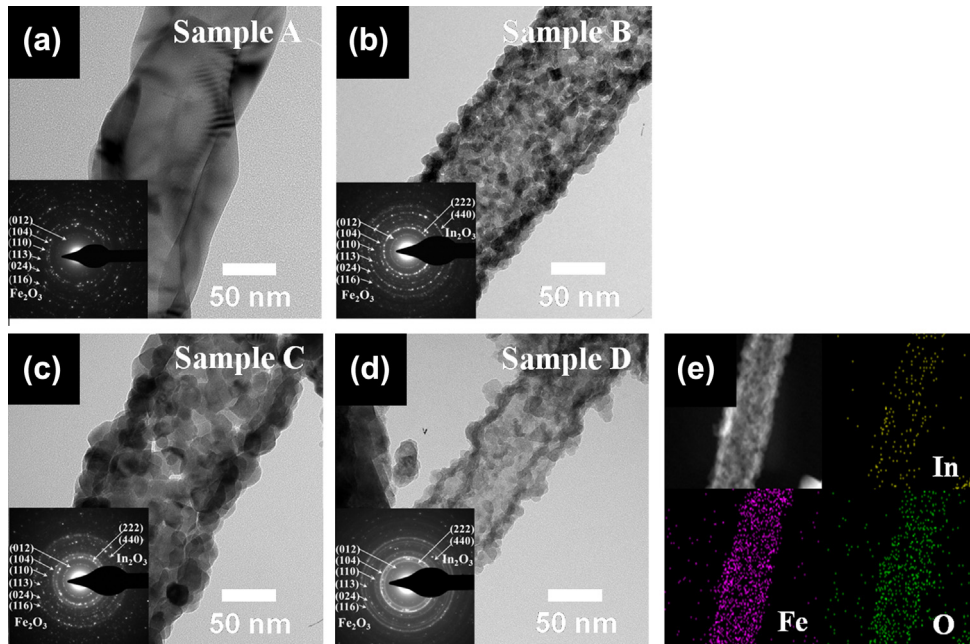


Fig. 3. (a)–(d) TEM images of samples A, B, C, and D, respectively. The insets show the SAED patterns for samples and (e) TEM-EDS mapping data for sample B.

nano-sized domains. The insets of Fig. 3(a)–(d) show the selected area electron diffraction (SAED) patterns for samples. The SAED patterns are composed of multiple ring and dot patterns. This indicates that the NFs are composed of nanoparticles with a well-defined crystalline structure. By indexing each ring patterns corresponding to the crystalline planes of the α -Fe₂O₃ and In₂O₃, we could conclude that the sample A is composed of one phase of Fe₂O₃ whereas the other samples are composed of mixed Fe₂O₃ and In₂O₃ phases. To investigate the compositional distribution in the NFs, elemental mapping for the In and Fe atoms was measured using an EDS system attached to the TEM for sample B, as shown in Fig. 3(e). Samples C and D showed similar SAED and EDS results as sample B (not shown here). This result shows that most of the Fe atoms were distributed widely at the surface, and the In atoms were gathered at the core of the NFs. Therefore, the structure of the NFs in samples B, C, and D, can be simplified, similar to the In₂O₃ core/Fe₂O₃ shell structures shown in a schematic illustration of Fig. 1(c). Also, morphological variations of the surface were observed among the samples. In particular, sample A exhibits a smooth surface, whereas other samples prepared using Fe and In precursors show a rough surface that is composed of tiny particles of various sizes. The average diameters of particles consisting of NFs are about 9 nm for sample B, 24 nm for sample C, and 9 nm for sample D. Thus, the observed particle size increased and decreased again with increasing the In/Fe molar ratio. These results are in good agreement with the SEM results and reveal that sample B consisted of ultrafine particles that were well-distributed on the NF surface as compared to other samples.

Fig. 4(a) shows XRD patterns of the samples after calcination. For sample A, the diffraction peaks at 24.1°, 33.1°, 35.6°, 40.8°, 49.5°, and 54.1° correspond to the (012), (104), (110), (113), (024), and (116) planes for the hematite α -Fe₂O₃ phase having rhombohedral structure (space group R3c [167]; JCPDS card no. 33-0664), respectively. Also, the sharp and strong peaks from sample A represent a high degree of crystallization of the α -Fe₂O₃ phase. For samples B, C, and D, however, the diffraction pattern is composed of peaks corresponding to the hematite α -Fe₂O₃ phase with additional peaks near 30.7° and 51.8°. The additional peaks correspond to diffraction peaks from the (222) and (440) planes

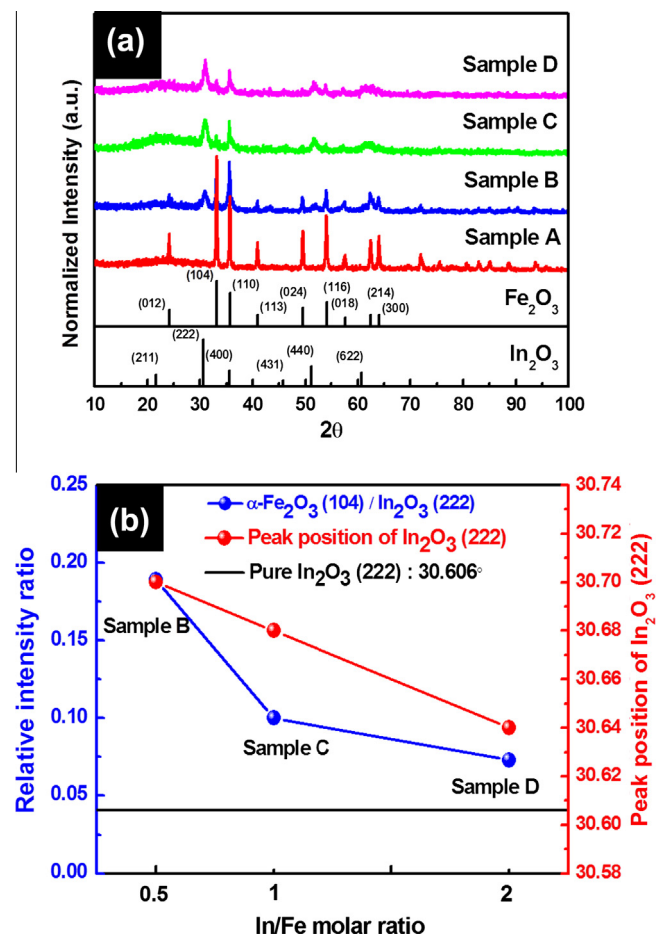


Fig. 4. (a) Normalized θ - 2θ XRD patterns of Fe-doped In₂O₃/ α -Fe₂O₃ core/shell NFs with variation of the Fe/In ratio and (b) relative intensity ratio between α -Fe₂O₃ (104) and Fe-doped In₂O₃ (222) peaks, and shift of the (222) peak position of In₂O₃ with variation of the Fe/In ratio.

of the bixbyite In_2O_3 phase with a cubic structure (space group Ia3 [206]; JCPDS card no. 06-0416). No diffraction peaks for any other chemical species, such as intermetallic compounds between Fe and In, were observed. The XRD results imply that $\alpha\text{-Fe}_2\text{O}_3$ and In_2O_3 phases coexisted in samples B, C, and D, whereas sample A was composed of a single $\alpha\text{-Fe}_2\text{O}_3$ phase. This result is consistent with the FE-SEM and TEM results. To further investigate the compositional evolution of the NFs, the relative peak intensity ratio of the main peaks of $\alpha\text{-Fe}_2\text{O}_3$ to In_2O_3 was plotted with respect to the variation of the In/Fe molar ratio, as shown in Fig. 4(b). The relative amount of the $\alpha\text{-Fe}_2\text{O}_3$ compared to that of In_2O_3 decreased with an increase in the In/Fe molar ratio up to a value of 2. Fig. 4(b) also shows the variations of the peak position of the (222) plane for the In_2O_3 phase with variations in the In/Fe molar ratio. The peaks for $\text{In}_2\text{O}_3/\alpha\text{-Fe}_2\text{O}_3$ core/shell NFs shifted slightly toward a higher angle than that of the pure In_2O_3 phase (the bixbyite structure). We attribute this to a decrease in the lattice size of the In_2O_3 matrix by incorporation of the Fe atoms because of the smaller ionic radius of Fe^{3+} (0.64 Å) compared to that of In^{3+} (0.80 Å) [22]. This indicates that the Fe element was doped into the In_2O_3 core materials by diffusion during heat-treatment. The incorporation of Fe^{3+} ions into the In_2O_3 lattice can enhance the magnetic properties of the In_2O_3 semiconductor by producing ferromagnetism. As the source In/Fe molar ratio was increased to 2, the diffraction peak positions shifted to a smaller angle approaching to that of the pure In_2O_3 . This would be due to that the strain in the In_2O_3 caused by the incorporation of a smaller Fe^{3+} ion (compared to the size of an In^{3+} ion) inhibited more incorporation of the foreign elements.

To investigate the chemical binding states of the elemental Fe and In in the NFs, XPS examinations were performed for all samples as shown in Fig. 5. The binding energies of the samples were corrected using the C 1s value of 284.5 eV. Fig. 5(a) shows that the XPS Fe $2p_{3/2}$ and Fe $2p_{1/2}$ core-level spectra for sample A are located at ~ 710.3 eV and ~ 723.9 eV, respectively. This indicates that elemental Fe is defined as an Fe^{3+} species, corresponding to the formation of the Fe_2O_3 phases. For samples B, C, and D (Fig. 5(b)–(d), respectively), the XPS Fe $2p$ spectra are divided into Fe^{3+} peaks and Fe^{2+} peaks. In particular, the presence of the Fe^{2+} species can be explained by the existence of oxygen vacancies that were near the Fe sites, which caused the slight shift toward higher angles compared to sample A. Also, this phenom-

non was confirmed by reports in the literature for the fabrication of Fe-doped In_2O_3 powders [23]. In addition, for the In $3d$ spectra of samples B, C, and D, the binding energies corresponding to In $3d_{5/2}$ and $3d_{3/2}$ were observed at ~ 444.1 and ~ 451.6 eV, respectively, indicating that elemental In exists in In^{3+} states, corresponding to the formation of the In_2O_3 phase. Thus, the XRD and XPS results indicate that the NFs are composed of Fe-doped $\text{In}_2\text{O}_3/\alpha\text{-Fe}_2\text{O}_3$ core/shell structures synthesized using co-electrospinning.

To investigate the magnetic properties of the In_2O_3 and $\alpha\text{-Fe}_2\text{O}_3$ core-shell NFs, we measured the magnetization with an applied magnetic field at 300 K. Fig. 6(a) shows representative magnetization versus magnetic field hysteresis loops for the samples. The pure $\alpha\text{-Fe}_2\text{O}_3$ NF, sample A, shows a negligibly weak magnetic property because $\alpha\text{-Fe}_2\text{O}_3$ exhibits an antiferromagnetic property below ~ 260 K and weak ferromagnetism between 260 K and the Néel temperature, 950 K. However, the In_2O_3 and $\alpha\text{-Fe}_2\text{O}_3$ core-shell NFs show enhanced magnetic properties compared to those of the pure $\alpha\text{-Fe}_2\text{O}_3$, depending on the In/Fe molar ratio. Fig. 6(b) summarizes the saturation magnetization (M_s) with variation of the Fe/In ratio. Sample B shows an abnormally large value of M_s , approximately 22.37 emu/g, which is about 47 times larger than that of sample A. With an increase in the In/Fe molar ratio up to 2, the M_s value decreased to 7.38 emu/g, which is still much higher than that of sample A. These large values of M_s for the In_2O_3 and $\alpha\text{-Fe}_2\text{O}_3$ core-shell NFs are assumed to be from the modification of the magnetic properties. We suggest three reasons for this enhanced magnetization of the In_2O_3 and $\alpha\text{-Fe}_2\text{O}_3$ core-shell structured NFs: (1) Fe doping into the In_2O_3 lattice, thereby resulting in the ferromagnetic property; (2) the size effect of the $\alpha\text{-Fe}_2\text{O}_3$ nanoparticles; and (3) 1-D core/shell structural advantages of the In_2O_3 supporting core and surrounding magnetic $\alpha\text{-Fe}_2\text{O}_3$ nanoparticles. If Fe atoms are doped into the In_2O_3 matrix, the non-magnetic In_2O_3 semiconductor can be a diluted magnetic semiconductor, resulting in enhanced magnetic properties [24]. Therefore, Fe doping into In_2O_3 can result in a large M_s value. Another mechanism for enhanced magnetism in the In_2O_3 and $\alpha\text{-Fe}_2\text{O}_3$ core-shell NFs is the size effect of the $\alpha\text{-Fe}_2\text{O}_3$ nanoparticles on the surface of NFs. Exchange energy inside the bulk $\alpha\text{-Fe}_2\text{O}_3$ lattice cancels the magnetic moment each other and results in a total magnetization of zero; *i.e.*, antiferromagnetism. However, the magnetic properties of $\alpha\text{-Fe}_2\text{O}_3$ nanostructures with a particle size of less than 1 μm have been known to be very sensitive to the size,

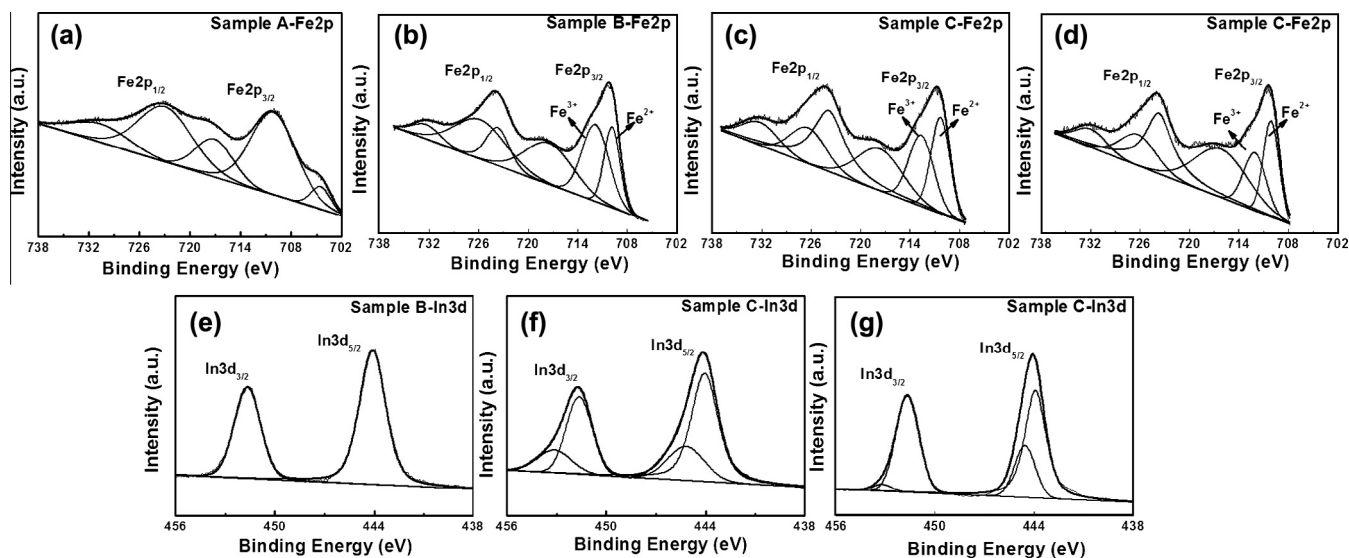


Fig. 5. XPS core-level spectra of (a) Fe $2p$ and (b) In $3d$ for samples A, B, C, and D.

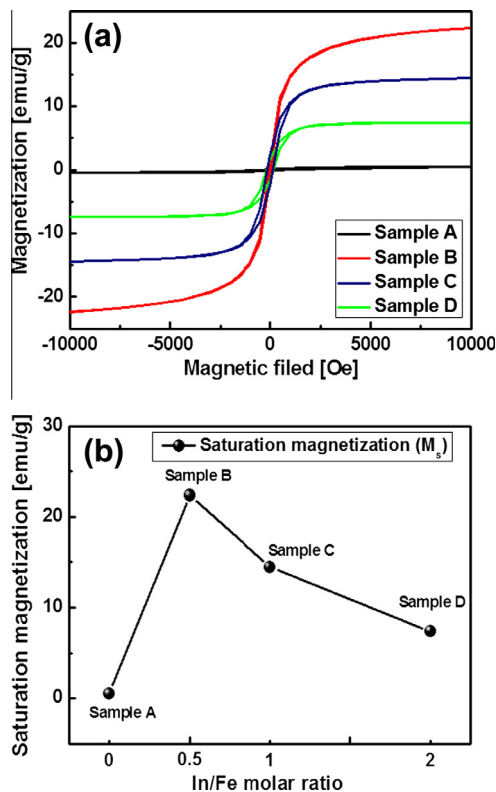


Fig. 6. (a) Magnetization versus field hysteresis loops for the samples and (b) summary of saturation magnetization (M_s) with variation of the Fe/In ratio.

dimensions, and morphology of the nanostructure [12,25,26]. It has been reported that the M_s value increases with a decreasing α -Fe₂O₃ particle size [12,25,26]. It should be noted that the α -Fe₂O₃ particle size on the surface of NFs is less than 1 μ m range, as shown in the TEM results. Sample B showed the smallest particle size and highest M_s value. This is consistent with the reported size effect on the magnetic properties of α -Fe₂O₃. Another mechanism for enhanced magnetism in the In₂O₃ and α -Fe₂O₃ core-shell NFs is a result of structural advantages of the In₂O₃ supporting core and surrounding magnetic α -Fe₂O₃ nanoparticles. The shape of the In₂O₃ and α -Fe₂O₃ core-shell NFs fabricated in this study can be simplified as shown in the schematic diagram in Fig. 1(c). The In₂O₃ NF core material supports the magnetic α -Fe₂O₃ nanoparticles that are attached on the surface of the NFs. The supporting material enhances the dispersion of the α -Fe₂O₃ nanoparticles by inhibiting agglomeration between the particles. Furthermore, this shape enhances the energy barrier that hinders the thermal rotation of the magnetic domains, thereby increasing the value of M_s . Therefore, our structure, the Fe-doped In₂O₃ and α -Fe₂O₃ core-shell NF, can enhance magnetic properties even though the proposed fabrication approach is a very simple.

4. Conclusion

We synthesized the Fe-doped In₂O₃/ α -Fe₂O₃ core/shell NFs successfully using the proposed co-electrospinning method. Structural

investigations using FE-SEM, TEM, and XRD measurements showed that the core material was the In₂O₃ phase, whereas the shell material was composed of crystalline α -Fe₂O₃ nanoparticles. The size of the Fe₂O₃ particles on the In₂O₃ core NF surface was less than 1 μ m. Interestingly, the XRD and XPS results showed that the Fe elements were incorporated into the In₂O₃ lattice, finally resulting in the modification of the magnetic properties of the In₂O₃. The magnetic properties of the Fe-doped In₂O₃/ α -Fe₂O₃ core/shell NFs showed abnormally strong magnetic properties and an increased value of M_s with an increased In/Fe molar ratio. We proposed three mechanisms for the enhanced magnetic properties of In₂O₃ and α -Fe₂O₃ core/shell structured NFs by Fe doping into an In₂O₃ lattice, thereby causing the ferromagnetic property, the size effect of the α -Fe₂O₃ nanoparticles, and the structural advantages of the In₂O₃ supporting core and surrounding magnetic α -Fe₂O₃ nanoparticles. Our results provide a simple and novel fabrication approach for Fe-doped In₂O₃/ α -Fe₂O₃ core/shell NFs with enhanced magnetic properties.

Acknowledgements

This research was supported by Basic Science Research Program through the National Research Foundation of Korea (NRF) funded by the Ministry of Education, Science and Technology (2012-007444 and 2012R1A1A1001711).

References

- [1] R. Dronskowski, *Adv. Funct. Mater.* 11 (2001) 27–29.
- [2] Y. Mizukoshi, S. Seino, T. Kinoshita, T. Nakagawa, T.A. Yamamoto, S. Tanabe, *Scr. Mater.* 54 (2006) 609–613.
- [3] J. Dobson, *Drug Dev. Res.* 67 (2006) 55–60.
- [4] J.A. Wiemann, E.E. Carpenter, J. Wiggins, W. Zhou, J. Tang, S. Li, V.T. John, G.J. Long, A. Mohan, *J. Appl. Phys.* 87 (2000) 7001–7003.
- [5] F. Bentivegna, M. Nyvlt, J. Ferré, J.P. Jamet, A. Brun, S. Visnovsky, R. Urban, *J. Appl. Phys.* 85 (1999) 2270–2278.
- [6] C. Holm, J.-J. Weis, *Curr. Opin. Colloid Interface Sci.* 10 (2005) 133–140.
- [7] E. Taboada, R. Solanas, E. Rodríguez, R. Weissleder, A. Roig, *Adv. Funct. Mater.* 19 (2009) 2319–2324.
- [8] S.K. Apte, S.D. Naik, R.S. Sonawane, B.B. Kale, J.O. Baeg, *J. Am. Ceram. Soc.* 90 (2007) 412–414.
- [9] I. Cesar, A. Kay, J.A.G. Martinez, M. Grätzel, *J. Am. Chem. Soc.* 128 (2006) 4582–4583.
- [10] J. Chen, L. Xu, W. Li, X. Gou, *Adv. Mater.* 17 (2005) 582–586.
- [11] B. Jia, L. Gao, *Cryst. Growth Des.* 8 (2008) 1372–1376.
- [12] D. Jagadeesan, U. Mansoori, P. Mandal, A. Sundaresan, M. Eswaramoorthy, *Angew. Chem. Int. Ed.* 47 (2008) 7685–7688.
- [13] J. Zhang, A. Thurber, C. Hanna, A. Punnoose, *Langmuir* 26 (2010) 5273–5278.
- [14] G.-H. An, H.-J. Ahn, *Carbon* 65 (2013) 87–96.
- [15] M. Angarano, S. Schulz, M. Fabritius, R. Vogt, T. Steinberg, P. Tomakidi, C. Friedrich, R. Mülhaupt, *Adv. Funct. Mater.* 23 (2013) 3277–3285.
- [16] C. Gualandi, A. Zucchelli, M.F. Osorio, J. Belcarì, M.L. Focarete, *Nano Lett.* 13 (2013) 5385–5390.
- [17] W. Pan, R. Han, X. Chi, Q. Liu, J. Wang, *J. Alloys Comp.* 577 (2013) 192–194.
- [18] W.-Y. Lee, H.-J. Yun, J.-W. Yoon, *J. Alloys Comp.* 583 (2014) 320–324.
- [19] Y.-J. Lee, H.-J. Ahn, *Ceram. Int.* 39 (2013) 5303–5308.
- [20] H. Dong, L. Sun, S. Sun, W. Xie, L. Zhou, X. Shen, Z. Chen, *Appl. Phys. Lett.* 97 (2010) 223114.
- [21] Z. He, Z. Chen, Y. Li, Q. Zhang, H. Wang, *Cryst. Eng. Commun.* 13 (2011) 2557–2565.
- [22] J. Yu, L.B. Duan, Y.C. Wang, G.H. Rao, *J. Solid State Chem.* 182 (2009) 1563–1569.
- [23] S. Yan, S. Ge, Y. Zuo, W. Qiao, L. Zhang, *Scr. Mater.* 61 (2009) 387–390.
- [24] G. Peleckis, X.L. Wang, S.X. Dou, *Appl. Phys. Lett.* 88 (2006) 132507.
- [25] A. Demortière, P. Panissod, B.P. Pichon, G. Pourroy, D. Guillon, B. Donnio, S. Bégin-Colin, *Nanoscale* 3 (2011) 225–232.
- [26] Y. Zhu, F.Y. Jiang, K. Chen, F. Kang, Z.K. Tang, *J. Alloys Comp.* 509 (2011) 8549–8553.